# G&G
# Lab Notes

**Editors**
Thomas M. Moses | Shane F. McClure

## Large Faceted Gem-Quality AFGHANITE

Afghanite is a blue mineral named in 1968 after its discovery in Badakhshan Province, Afghanistan. It is often found in association with lapis lazuli and sodalite (R.V. Gaines et al., *Dana's New Mineralogy*, John Wiley & Sons, New York, 1997, p. 1634). It has a chemical formula of $(Na,Ca,K)_8(Si,Al)_{12}O_{24}(SO_4,Cl,CO_3)_3 \cdot H_2O$ (Gaines et al., 1997). Since 2003, there have been only a few mentions in the literature of gem-quality afghanite (Winter 2003 GNI, pp. 326–327; Spring 2008 GNI, pp. 79–80; Fall 2011 GNI, p. 235; Spring 2015 GNI, p. 83), with no reports of finished faceted stones larger than 1.5 ct. Five gem-quality samples ranging in size from 2.87 to 7.25 ct have been reported; however, all five were cabochons and contained numerous inclusions of lazurite (Winter 2003 GNI, pp. 326–327).

For these reasons, the 1.91 ct transparent faceted oval brilliant afghanite recently submitted to the Carlsbad lab for an identification report was truly exceptional (figure 1). The only inclusions in the stone were minor fractures. To date, it is the largest facet-grade afghanite on record in the GIA gem identification department. Standard gemological testing revealed

*Figure 1. An exceptionally large and clean 1.91 ct faceted oval brilliant afghanite was recently submitted to GIA's Carlsbad lab.*

that the stone was doubly refractive and uniaxial, with an RI of 1.522 to 1.530 and a specific gravity (SG) of 2.52. These results are consistent with the published properties of afghanite (Gaines et al., 1997). Additionally, an early report on gem-quality afghanite notes that "an interesting feature of afghanite that should prove useful in its identification is its strong, bright orange fluorescence to long-wave UV radiation," a property that this remarkable stone exhibited (Winter 2003 GNI, p. 326–327). Further confirmation of the stone's identity was obtained by using Raman spectroscopy, which yielded a spectrum that matched that of known afghanite samples.

*Hollie McBride*

## BERYL and Glass Assemblage Imitating Emerald

Assemblages of various materials have long been used as imitations of precious stones, with records dating back to Pliny the Elder's *Natural History* (79 AD). Assembled stones commonly consist of two or more pieces of materials joined together in a parallel, layered fashion. Natural gem materials, such as spinel or garnet, are often used for the crown for the dual benefit of their durability and natural inclusions. The pavilion is typically composed of attractively colored, inexpensive materials such as glass or synthetic sapphire.

A unique assembled 3.35 ct imitation emerald composed of five glass segments surrounding a rectangular beryl core (figure 2) was submitted to the New York lab. Microscopic observation revealed multiple nonparallel cement planes in the pavilion (figure 3, left). The crown was shown to be separated from the pavilion in a single piece, whereas the pavilion was composed of four asymmetrical exterior segments surrounding a sub-rectilinear pyramidal core. The core material contained inclusions typical of natural beryl, such as dark dendritic flakes (figure 3, right) and fingerprints. Large gas bubbles and internal chips were observed within the cement layers that accumulated at the beryl core's corners. Standard gemological testing produced consistent RIs of 1.61 on both the crown and the four segments that made up the pavilion, an SG of 2.99, and weak white fluorescence in the cement planes in long- and short-wave UV light. Under cross-polarized light,

Figure 2. Face-up, the assemblage displayed natural inclusions underneath the table. Large bubbles are also visible at the corners of the beryl core, a warning sign for the observant viewer.
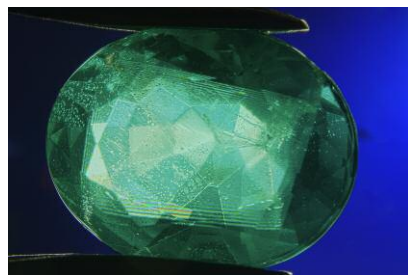


Figure 3. Left: All four glass sections of the pavilion assemblage are visible in reflected light. The small triangular segment is a protrusion from the opposite side. Field of view 3.57 mm. Right: Metallic dendritic films supporting the natural provenance of the beryl core. Also visible are planar bubbles within the cement layer. Field of view 2.90 mm.

the outer material was singly refractive and displayed interference patterns along the interior join planes (figure 4). When immersed, the coloration was shown to be derived from the surrounding sections and joined by a colorless cement. This was further supported by ultraviolet/visible/near-infrared (UV-Vis-NIR) spectroscopy, which yielded a spectrum similar to manufactured green glass samples from our database. Raman microscopy of the crown and four pavilion segments produced amorphous spectra typical of glass. In addition to amorphous mounds, beryl peaks were detected in the core material, confirming prior suspicions.

Interestingly, the four glass segments in the pavilion assemblage are interlocked in a fashion that reveals a possible explanation of how the stone was manufactured. Based on visual observations, it appears the pavilion was constructed by a laborious multi-step cut-and-glue process (figure 5). As a result of the iterant cutting, the first segment shares five sides that are parallel to the faces of the beryl core (four pyramidal faces and one basal). The number of faces parallel to the core decreases by one for each added glass segment. The asymmetry of the segments, parallel faces, and precise angles that match the sides of the core support the proposed model of ordered assembly.

Figure 4. Face-up view under cross-polarized light displaying the inert reaction of the outer material and interference planes outlining the beryl core. Field of view 14.52 mm.



Figure 5. Diagram showing the proposed model of the complex assembly of the composite stone. Final faceting is shown for simplicity. A: The first glass segment (green) is attached to the beryl core (gray). B: Both the core and the first segment are cut to make a flat surface for the second segment. C: The second segment (teal) is attached. D: The segments are again cut. E: The third segment (blue) is attached. F: The assemblage is shown rotated 180° for clarity. All current pieces are cut to create the surface for the final piece. G: The fourth and final segment (purple) is attached. H: Omitted for simplicity, the assembled pavilion would likely be polished flat to make room for the crown. Lastly, the crown (pink) is attached. The diagram was generated using Onshape CAD software.
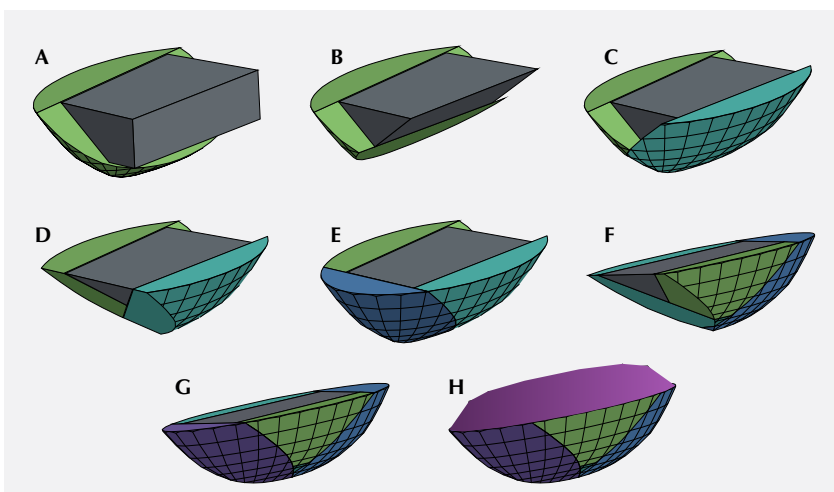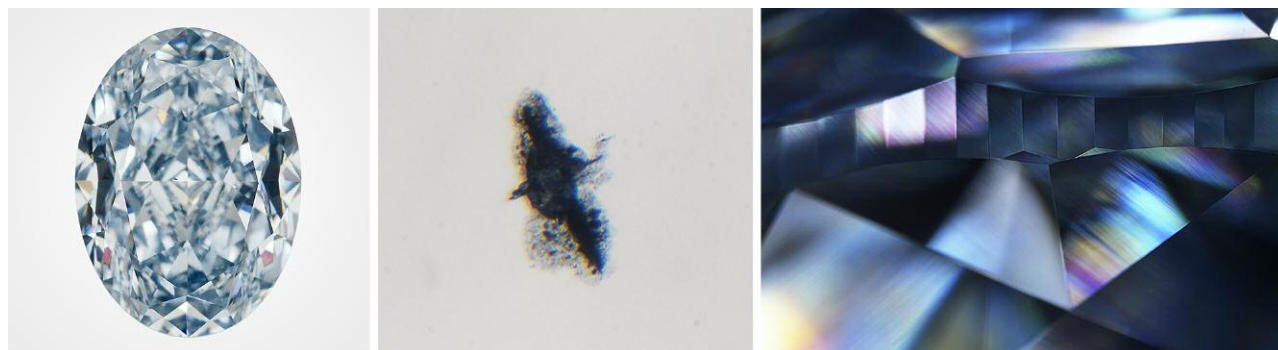
Figure 6. This 17.09 ct HPHT-treated blue diamond (left) has ragged-looking graphitization around an inclusion (center, field of view 0.76 mm) and high-order interference colors when viewed with crossed-polarizing filters (right, field of view 7.19 mm).

The authors were not able to find any records of this type of assembled stone, and it was the first time one has been submitted to GIA's New York or Carlsbad laboratories. Since all exposed surfaces were glass, it is assumed that the stone was fabricated relatively recently due to the sharp facet junctions and lack of wear. It is intriguing that an antiquated technique is updated in modern times, serving as a cautionary tale of the ingenuity counterfeiters employ.

*Tyler Smith and Augusto Castillo*

## Large HPHT-Treated Blue Type IIb DIAMOND

Over the past two decades, high-pressure, high-temperature (HPHT) treatment has emerged as a prominent technology for changing the color of diamonds. It is best known for removing brown coloration from natural type IIa material to yield colorless or, rarely, pink diamonds. Similarly, HPHT treatment can be used to reduce the brown color component of gray or brownish natural type IIb (boron-bearing) diamonds, thereby increasing the underlying blue color. Improvements to equipment and methods continue to push the capabilities of HPHT processing.

GIA's New York lab recently encountered a notably large HPHT-treated Fancy Intense blue oval-cut diamond (figure 6, left). At 17.09 ct, this is the largest HPHT-treated blue diamond graded by GIA to date. For comparison, the average size of most submitted HPHT-processed blue diamonds lies in the 1 to 5 ct range. HPHT treatment can be challenging to detect with standard gemological tools, but in this case the ragged-looking graphitization around an inclusion and the appearance of moderate to high-order interference colors under crossed polarizers were helpful clues (figure 6, center and right). Advanced testing methods (e.g., infrared spectroscopy and photoluminescence spectroscopy) confirmed that the stone was HPHT treated.

Additionally, this diamond had a striking blue color zonation (figure 7, left) that is thought to be unrelated to HPHT treatment. A region of strong blue color is separated from an almost colorless region by a sharp division with octahedral plane {111} orientation. Color zonation is not uncommon in natural type IIb diamonds, though it is seldom so sharp and planar (J.M. King et al., "Characterizing natural-color type IIb blue diamonds," Winter 1998 *G&G*, pp. 246–268). The stronger blue region likely contains more uncompensated boron. It also exhibits more intense greenish blue fluorescence/phosphorescence in Diamond-View images (figure 7, right). The color boundary might reflect a change in defect incorporation during diamond growth.

*Evan M. Smith, Paul Johnson, and Kyaw Soe Moe*

## One Natural Melee Diamond Found in Large Batch of HPHT Synthetic Melee

Over the last decade, the production methods used to create synthetic dia-

Figure 7. Color zonation (left) becomes more noticeable when viewed through the pavilion. The stronger blue-colored region corresponds with bright greenish blue fluorescence in the DiamondView (right, field of view 5.8 mm). Note that the DiamondView image is taken from the opposite side of the diamond.
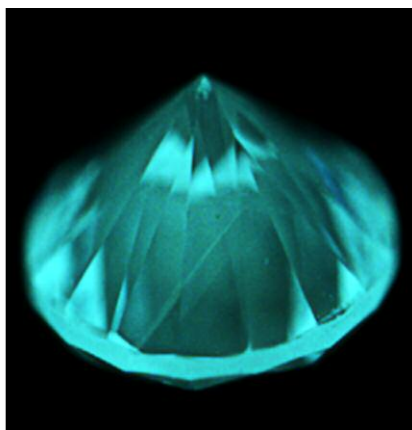
*Figure 8. Out of a parcel of 1,102 diamond melee received at GIA's New York lab for testing, 1,092 were identified as HPHT synthetic melee.*

mond melee have improved substantially, along with the quality of the specimens themselves. The increase in the amount of synthetic melee submitted—both disclosed and undisclosed—to GIA's laboratories for identification has exponentially increased since GIA began offering its Melee Analysis Service in 2016. Parcels of melee are often submitted with a mixture of naturals and synthetics. Typically, a few synthetics are detected in batches of natural melee diamonds, known in the trade as "salting" (e.g., S. Eaton-Magaña and J.E. Shigley, "Observations on CVD-grown synthetic diamonds: A review," Fall 2016 *G&G*, pp. 222–245).

GIA's New York laboratory received a batch of 1,102 melee diamonds with a total weight of 9.67 carats for the melee analysis service.

The tested melee ranged from 0.98 to 1.52 mm in diameter. Preliminary testing using GIA's fully automated screening device referred 1,093 for further testing, while nine were found to be outside of the service criteria. Further analysis using detailed spectroscopic analysis confirmed 1,092 (figure 8) out of the 1,093 to be HPHT synthetics. Fourier-transform infrared (FTIR) absorption spectroscopy performed on the referred melee revealed an absorption band at approximately 2800 cm$^{-1}$ from trace boron in the diamond lattice, classifying these melees as type IIb (boron-bearing), typical of HPHT synthetic diamonds. Due to the relatively high concentrations of boron, these melee diamonds showed a clear blue hue, which is very different from most of the melee diamonds we have tested.

Further examination using photoluminescence (PL) spectroscopy showed no detectable peaks of nickel, often a catalyst used to grow HPHT synthetic diamonds (e.g., Spring 2017 Lab Notes, pp. 95–96). These spectra were in fact atypical of HPHT synthetic diamonds. Distinctive HPHT growth patterns were observed in the DiamondView (figure 9) along with strong phosphorescence following exposure to short-wave UV radiation (figure 10).

One sample out of 1,093 was confirmed as a natural diamond. Infrared absorption spectroscopy indicated this stone was type Ia, with a hydrogen peak at 3107 cm$^{-1}$. DiamondView imaging displayed a typical blue fluorescence and no detectable phosphorescence, both typical for a natural type Ia diamond.

It is interesting to note that only one natural was found in this parcel of melee. This has been the largest percentage of undisclosed synthetic melee that GIA has seen. The majority of the HPHT synthetic melee had no detectable traces of Ni, demonstrating the importance of advanced testing to identify these melees.

*Stephanie Persaud, Wuyi Wang, Paul Johnson, and Ivana Petriska Balov*

*Figure 10. These HPHT-grown synthetic diamond melee, from the parcel of 1,102 specimens, display strong phosphorescence following exposure to short-wave UV radiation.*

*Figure 9. This diamond shows characteristic growth patterns of HPHT-grown material.*

### A Repaired Diamond

A 1.38 ct marquise-cut diamond (figure 11) was submitted to the Carlsbad lab for colored diamond grading services. It was initially noted that large fractures and a large cavity were present on the table. Careful examination of the stone with a gemological microscope revealed that it had previously broken in half and been repaired with an unknown adhesive. The first clue was a large fracture from the crown to the pavilion that showed a sizeable gap present throughout the stone. Furthermore, the facets the fracture passed through all showed slight to moderate misalignment, which cannot happen during polishing (figure 12). Finally, large trapped air bubbles could be seen in the fracture when viewed at an angle. These clues proved that the diamond had broken and been put back together again, though not perfectly. Polish lines on the pavilion facets showed a pattern that would line up if not for the fracture separating them, demonstrating that the breakage occurred after the diamond had been at least partially polished. Beyond that, it is impossible to tell when the damage occurred.



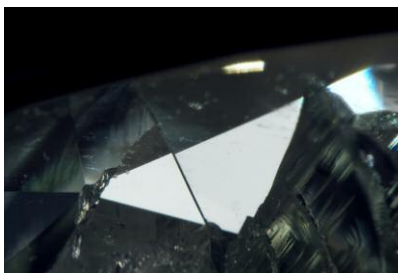Figure 11. A face-up photo of the repaired diamond.



*Figure 12. A bezel facet of the repaired diamond as seen in reflected light. The wide fracture can be seen cutting across the facet, and the upper edge of the facet does not form a straight line. Field of view 3.3 mm.*

Diamonds have been adhered together with glue to form a diamond-diamond doublet (E. Barrie and E. Biermans, "A different type of deception: 'Diamond-diamond' doublet," HRD Antwerp, 2014, www.hrdantwerp.com/en/news/a-different-type-of-deception-diamond-diamond-doublet), but a broken diamond that has been repaired was not something previously reported by GIA. The fracture in the item was not a flat, straight surface but very irregular, indicating that it was not two separate diamonds glued together to make a larger diamond, but rather a repair. Since the item was simply two pieces of diamond joined together, it was not eligible to receive a diamond grading report. None of the 4Cs apply to a composite such as this (e.g., the carat weight of the item was actually the sum of the weights of two diamonds plus the weight of the adhesive). The decision to repair a diamond in this manner is unusual. Careful gemological examination will, however, reveal the repair work done.

*Troy Ardon*

### A Cat's-Eye Rock Consisting of JADEITE and Amphibole

The Hong Kong laboratory recently examined a translucent variegated green bead exhibiting chatoyancy (figure 13). The 1.42 ct bead, measuring approximately 5.62 mm in diameter, displayed two different shades of green on opposite sides. A distinct cat's-eye band was readily visible across the darker green region with fiber-optic illumination, whereas no chatoyancy was observed in the lighter green region on the reverse side.

Microscopic observation revealed that the darker green side consisted of parallel fibrous crystals (figure 14, left). Light reflecting off these oriented crystals produced a chatoyant band perpendicular to the length of the



*Figure 13. This 1.42 ct translucent variegated green bead displays a distinct chatoyant band on the darker green side (left). No chatoyancy was observed on the lighter green side (right).*
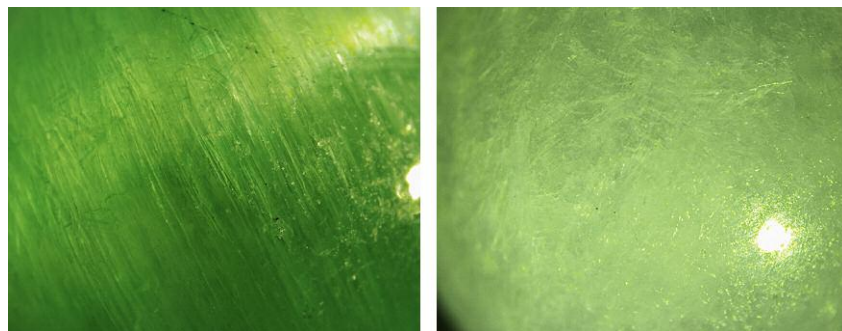
Figure 14. Left: Parallel fibrous amphibole crystals were the cause of chatoyancy in this green bead; field of view 11.34 mm. Right: Tight interlocking grains were visible in the lighter green jadeite region; field of view 3.80 mm. Both observed with fiber-optic illumination.

crystals. On the lighter green side, tight interlocking grains were observed (figure 14, right). Raman spectroscopy detected the presence of richterite, an amphibole with the general formula $Na_2CaMg_5Si_8O_{22}(OH)_2$, in the darker green region and jadeite in the lighter green region.

While it is not unusual to encounter a rock consisting of jadeite and amphibole (G. Shi, "Mineralogy of jadeitite and related rocks from Myanmar: a review with new data," *European Journal of Mineralogy*, Vol. 24, No. 2, 2012, pp. 345–370), it is fascinating to see such a rock being fashioned into an attractive variegated green bead exhibiting chatoyancy.

*Bona Hiu Yan Chow*

## Two Natural "Horse Conch" PEARLS

GIA's Hong Kong laboratory recently examined two strongly saturated red-dish orange non-nacreous pearls weighing 126.20 ct and 4.89 ct, and measuring 40.80 × 23.70 × 20.96 mm and 10.53 × 8.55 × 7.68 mm, respectively. The client who submitted the pearls also provided the shell from which they were reportedly extracted (figure 15). While such information must be treated with a degree of caution, our client also stated that the shell and pearls were handed to him by a fisherman who claimed to have found them in the waters off Isla Mujeres, near Cancun, Mexico. The shell measured approximately 47 × 24 × 24 cm and appeared pinkish orange with an orangy brown periostracum. Its large size, characteristic shape, pinkish orange color, and fine slender flame structures enabled us to identify it as a member of the *Triplofusus* genus, most likely *Triplofusus papillosus* or *Triplofusus giganteus*, sometimes referred to as *Pleuroploca gigantea* (E. Strack, *Pearls*, Rühle-Diebener-Verlag GmbH & Co., Stuttgart, Germany, 2006, p. 108; Fall 1994 Lab Notes, p. 195). These are all names that have been used to describe the Florida horse conch, though differences of opinion on the correct nomenclature applicable exist (D.P. Berschauer, "What's in a name – the Florida horse conch," *The Festivus*, Vol. 49, 2017, pp. 110–116). The *Triplofusus* genus is part of the Fasciolariidae subfamily which is a very diverse group of marine gastropods. The parallel line patterned *Pleuroploca trapezium* is another member of the Fasciolariidae subfamily said to produce unusual horse conch pearls (H. Bari and D. Lam, *Pearls*, Skira Editore S.p.A, Milan, 2009, pp. 70–73).

The larger of the two pearls displayed an uneven coloration with some lighter areas blending into a more saturated reddish orange. The smaller pearl was more homogeneous in appearance. The flame structures appeared spiky on the smaller pearl but were fine and elongated on the larger pearl (figure 16). Real-time microradiography revealed small void-like features in the center of the smaller pearl and toward the tapered

Figure 15. Two natural "horse conch" pearls and the shell from which they were reportedly extracted.
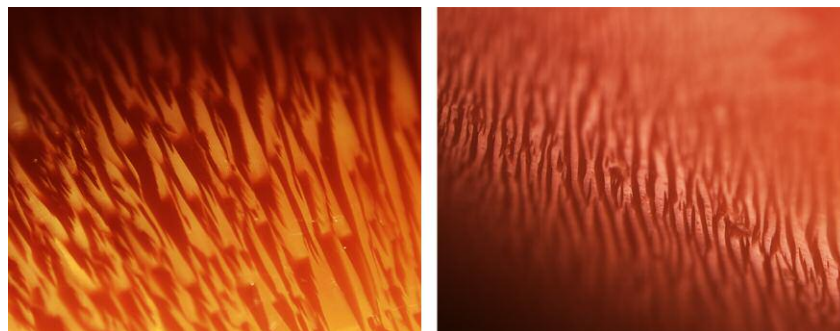
Figure 16. Short spiky flame structure on the 4.89 ct pearl (left, field of view 3.74 mm), and fine, elongated flame structure on the 126.20 ct pearl (right, field of view 2.83 mm).

end of the larger pearl. Such voids are not uncommon in the pearls of a number of porcelaneous pearl-producing mollusks. GIA has recorded similar features in examples from species of *Tridacna/Hippopus*, *Strombus gigas*, *Cassis*, and *Melo*. While the flame structures bore some similarities to those seen in *Strombus gigas* (conch) pearls, their strong reddish orange color and internal structures aligned more closely with horse conch pearls. Raman spectroscopy using 514 nm laser excitation detected aragonite peaks at 702, 706, and 1086 cm$^{-1}$, as well as peaks at 1130 and 1520 cm$^{-1}$ attributed to naturally occurring polyenic pigments responsible for the strong reddish orange color. The natural coloration was further supported by the presence of numerous polyenic-related peaks in the PL spectrum (figure 17) collected with the same laser excitation.

Figure 17. The PL spectrum of the 4.89 ct horse conch pearl displayed numerous peaks associated with naturally occurring polyenic pigments.
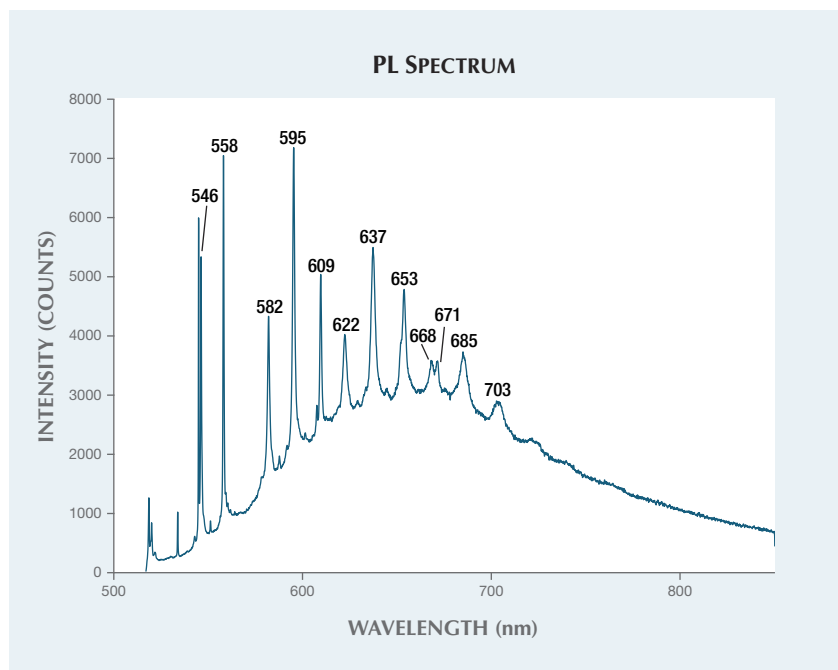


Although GIA handles a wide range of pearls originating from different mollusk species, horse conch pearls are among the rarest examined. It was, therefore, very rewarding to handle the 126.20 ct pearl and its smaller partner together with the shell from which they reportedly originated.

*Bona Hiu Yan Chow*

## Unique Star SAPPHIRE with Transparent Core

GIA's Tokyo laboratory recently examined a 34 ct oval cabochon of unique appearance. This cabochon consisted of a transparent yellow pseudohexagonal core in an opaque metallic-looking area (figure 18). Spot RIs on both areas were 1.76, and SG was 4.04. This appearance of a transparent yellow window with an opaque metallic surrounding area is reminiscent of pallasitic peridot, an olivine nodule enclosed in nickel-ion alloy of stony-iron meteorites (see J. Sinkankas et al., "Peridot as an interplanetary gemstone," Spring 1992 *G&G*, pp. 43–51). However, no surface discontinuity between these two parts can be found with close observation under reflected light. Furthermore, this metallic-looking area exhibited

Figure 18. This 34 ct sapphire cabochon has a yellow pseudohexagonal window surrounded by metallic-looking material that displays asterism.
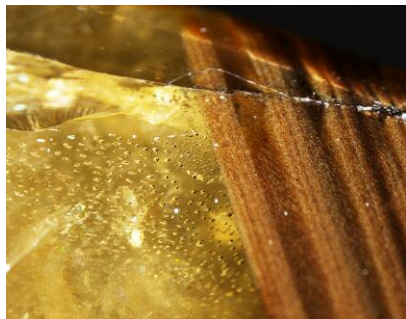
*Figure 19. The sapphire's yellow core includes negative crystals and healed fissures (left) and the metallic-looking part (right) has dense needles. Field of view 3.38 mm.*

six-rayed asterism. Under the microscope, negative crystals in a plane and healed fissures were found in the transparent area; densely packed needle-like inclusions, some crystals, and stained fissures were seen in the opaque area (figure 19). In addition to the microscopic observations, advanced testing of the yellow part revealed that this specimen was a natural corundum. The metallic appearance and asterism were caused by the strong reflection from the dense needle-like inclusions (figure 19), some of which were flat. These needles were identified as hematite and ilmenite by Raman spectroscopy. The slightly elevated SG of this specimen might have been caused by the abundance of these inclusions, since the SGs of both hematite and ilmenite are higher than that of corundum.

As previously documented (e.g. T.N. Bui et al., "From exsolution to 'gold sheen': A new variety of corundum," *Journal of Gemmology*, Vol. 34, No. 8, 2015, pp. 678–691; N. Narudeesombat et al., "Golden sheen and non-sheen sapphires from Kenya," Gem and Jewelry Institute of Thailand, July-August 2016, pp. 282–288; Winter 2016 Lab Notes, pp. 413–414), sapphires with golden shimmer caused by hematite needles are known as "golden sheen" or "Zawadi" sapphires in the trade. As with rutile needles in common star sapphires, hematite needles intersecting at 60 degrees can cause six-rayed asterism. Golden sheen sapphires sometimes have densely included parts, but such a distinct zoning of transparent and densely included parts has not been documented. This unique appearance may indicate a certain crystallizing condition of sapphires.

*Yusuke Katsurada*

## Cabochons Fashioned from the SHELL of *Crassostrea Virginica*

*Crassostrea virginica*, the so-called Eastern or American oyster, is a commercial seafood widely distributed along the east coast of the United States to the Gulf of Mexico ("Indian River Lagoon Species Inventory," Smithsonian Marine Station at Fort Pierce, 2008, https://www.sms.si.edu/irlspec/Crassostrea_virginica.htm). Connecticut, Virginia, and Mississippi have all designated the Eastern oyster as their official state shell, and cabochons cut from this bivalve are the official state gemstone of Louisiana (http://legis.la.gov/Legis/Law.aspx?d=103557). These specimens are marketed under the trade name La-Pearlite.

The Carlsbad laboratory received ten LaPearlite cabochons together with a shell for examination (figure 20). The cabochons exhibited low domes and flat bases and ranged from 1.65 to 6.12 ct. They measured from $6.85 \times 6.60 \times 3.80$ mm to $14.40 \times 10.30 \times 5.30$ mm and possessed non-nacreous surfaces, with the majority displaying a natural brownish yellow banded structure typical of shell formation. Microscopic examination revealed that the main white surface and subsurface structure varied from a patchwork of nondirectional cells or segments to a broad mottled appearance within individual specimens, as well as from specimen to specimen.

*Figure 20. The ten cabochon-cut gems examined are shown alongside the valves of* C. virginica *(Eastern or American oyster). The interior and exterior valves shown belong to one oyster. Samples courtesy of Anne Dale.*

*Figure 21. Left: A 3.09 ct cabochon showed various surface structures consisting of a non-directional patchwork of cells near the center to a broad mottled appearance in the outer area, together with natural brownish layers of shell formation. Right: Higher magnification of another cabochon's surface revealed a distinct patchwork structure. Both samples displayed a whitish sheen on the surface when illuminated with a fiber-optic light. Fields of view 11.90 mm (left) and 5.24 mm (right).*

These structures exhibited a reflective whitish sheen when illuminated by a fiber-optic light or other bright oblique lighting, creating a shimmery phenomenon (figure 21). A similar patchwork pattern has been noted on scallop pearls and shells of the Pectinidae family (K. Scarratt and H.A. Hänni, "Pearl from the lion's paw scallop," *Journal of Gemmology*, Vol. 29, No. 4, 2004, pp. 193–203). Under longwave UV radiation (365 nm), the white portions of all the cabochons and the shell were inert, while the yellow portions showed a weak to moderate yellow fluorescence, and the shell's dark purple adductor muscle scar exhibited a weak red fluorescence.

Raman spectroscopic analysis with a 514 nm argon-ion laser subsequently verified that the white and yellow portions of the cabochons and shell were calcite with peaks at 280, 712, 1085, and 1437 cm⁻¹. No peaks indicating the possible presence of pigments were detected in the yellow areas. Moreover, Raman spectra collected on the shell's dark purple adductor muscle scar produced aragonite peaks at 703 and 1085 cm⁻¹ along with several relatively weak broad pigment-related bands (figure 22). PL spectra collected with 514 nm laser excitation on the same areas showed clear triple bands at approximately 620, 650, and 680 nm (figure 23). The PL spectra and fluorescence reaction indicate the purple color is associated with the pigment porphyrin (Y. Iwahashi and S. Akamatsu, "Porphyrin pigment in black-lip pearls and its application to pearl identification," *Fisheries Science*, Vol. 60, No. 1, 1994, pp. 69–71;

L.H. Arma et al., "Red fluorescence lamellas in calcite prismatic layer of *Pinctada vulgaris* shell (Mollus, bivalvia)," *Optical Materials Express*, Vol. 4, No. 9, 2014, pp. 1813–1823). None of the studied cabochons showed purple areas to examine for comparison. Interestingly, the Raman spectra obtained from the white and purple areas of the same mollusk that were previously referenced in the literature (K. Scarratt et al., "A note on a pearl attached to the interior of *Crassostrea virginica* (Gmelin, 1791) (an edible oyster, common names, American or Eastern oyster)," *Journal of Gemmology*, Vol. 30, No. 1/2, 2006, pp. 43–50) differed slightly from the findings in this work. The samples in this submission were also analyzed by energy-dispersive X-ray fluorescence (EDXRF) chemical analysis and showed low levels of manganese (Mn), confirming their saltwater environment.

As with all shell mollusks, *C. virginica* is capable of producing pearls. However, the cabochons in this study provided useful gemological and spectroscopic information for future refer-

*Figure 22. Raman spectra collected using 514 nm laser excitation on the white and purple areas of the interior of the* C. virginica *valve. The white area shows calcite peaks at 280, 712, 1085, and 1437 cm⁻¹, and the purple area shows aragonite peaks at 703 and 1085 cm⁻¹, along with several broad pigment-related bands.*



RAMAN SPECTRA
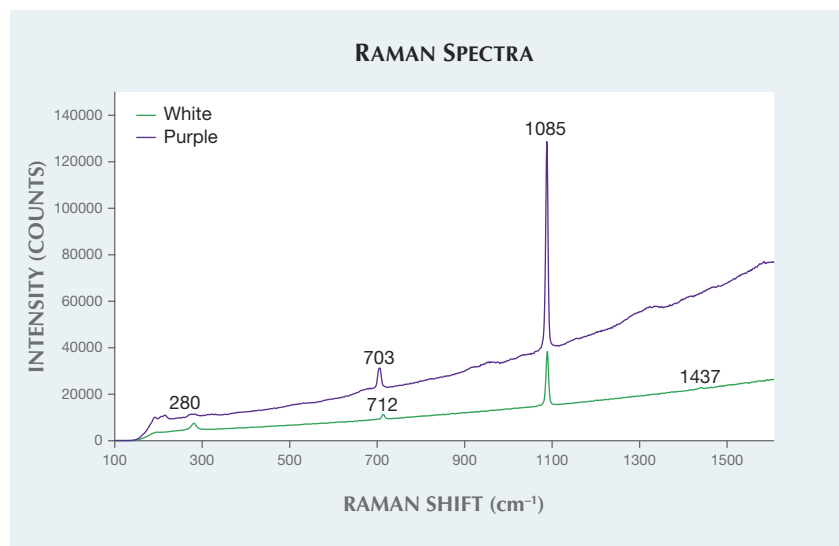
## PL SPECTRUM

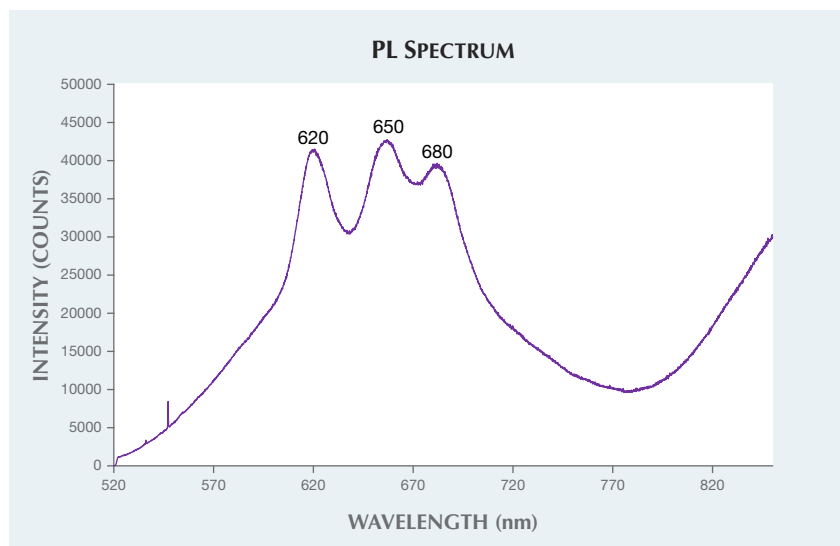Figure 23. A PL spectrum collected using 514 nm laser excitation on a purple area on the interior of a C. virginica valve displays clear triple bands at approximately 620, 650, and 680 nm related to the porphyrin pigment.
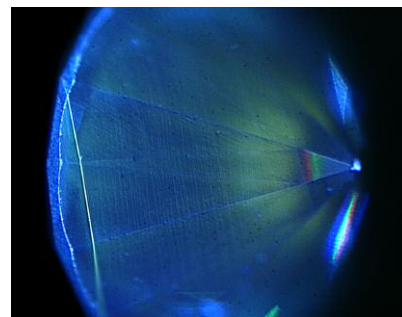


Figure 25. All three irradiated CVD synthetics displayed very weak fluorescence in the DiamondView, as seen in the 1.14 ct sample shown here. All showed the characteristic striations of CVD growth.

ence that can no doubt assist with identifying the composition of pearls produced by the mollusk (C.P. Idyll, "The pearls of Margarita," *Americas*, Vol. 19, No. 8, 1967, pp. 8–14). Although the samples could be mistaken for agate at first glance, owing to their distinctive banding, it would soon be apparent that they were pieces of fashioned shell. The samples demonstrate how creative work can turn nature's beauty into an attractive gemological material.

*Artitaya Homkrajae*

### Three Irradiated CVD SYNTHETIC DIAMONDS

While laboratory-irradiated diamonds are often submitted for grading reports, irradiated synthetics with a green-to-blue color are still a rare occurrence. Before the submissions described here, GIA's laboratory had examined only three irradiated CVD synthetics (Fall 2014 Lab Notes, pp. 240–241; Fall 2015 Lab Notes, pp. 320–321) and two irradiated HPHT synthetics. So it was interesting when the Carlsbad laboratory received three

irradiated CVD synthetics, apparently from the same client.

All three synthetics showed very similar features in terms of color (equivalent to Fancy Deep green-blue; figure 24), clarity (equivalent to $VVS_2$), and weight (1.12 ct, 1.14 ct, and 1.34 ct), along with comparable features detected by fluorescence imaging (figure 25) and spectroscopy (figure 26).

The Vis-NIR and IR absorption spectroscopy and the PL spectroscopy were nearly identical among the three specimens, indicating that they were probably grown and treated under similar if not identical conditions. The IR

Figure 24. These 1.12 ct, 1.14 ct, and 1.34 ct laboratory-irradiated CVD synthetic diamonds all have similar appearance, with color grades equivalent to Fancy Deep green-blue.
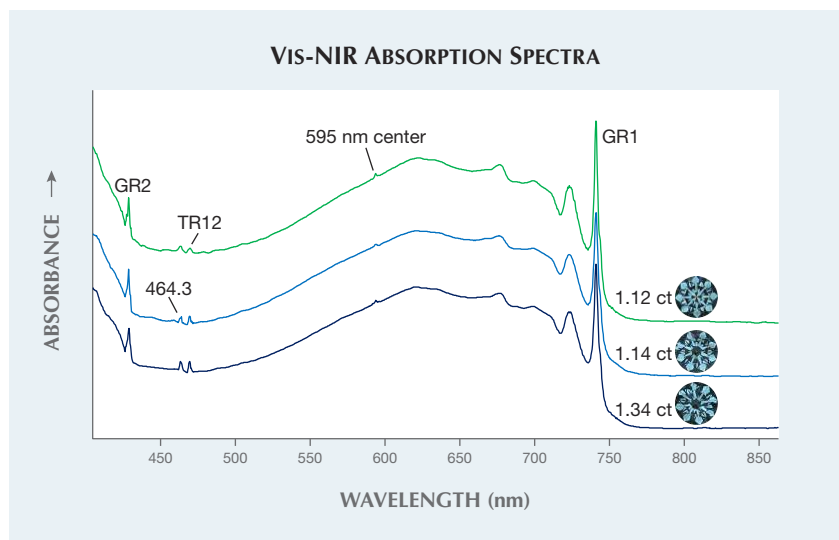
**Vis-NIR Absorption Spectra**

*Figure 26. Radiation-related features dominate the CVD synthetic diamonds' Vis-NIR absorption spectra when collected at liquid nitrogen temperature. Features include the GR1 at 741.2 nm, the 595 nm center at 594.2 nm, the TR12 center at 469.9 nm, a radiation-related peak at 464.3 nm, and the GR2 at 429 nm.*

absorption spectra showed very weak 3107 cm$^{-1}$ and 1344 cm$^{-1}$ peaks. Based on the integrated area of the 1344 cm$^{-1}$ peaks (I. Kiflawi et al., "Infrared absorption by the single nitrogen and A defect centres in diamond," *Philosophical Magazine B*, Vol. 69, No. 6, 1994, pp. 1141–1147), we determined the single N concentration as about 0.4–0.5 ppm for all three samples. The Vis-NIR absorption spectra showed typical features for irradiated diamonds: the TR12 (a radiation-related feature tentatively ascribed to a divacancy/di-interstitial defect at 469.9 nm), the 595 nm center, and GR1 [V$^0$] at 741.2 nm (figure 26). PL spectra showed a weak SiV$^-$ doublet at 736.6 and 736.9 nm along with a very strong GR1 center. PL spectroscopy also indicated the presence of the H2 peak at 986.2 nm and the lack of the 596/597 nm doublet that is normally seen in as-grown CVD synthetics and generally disappears with post-growth treatment. This combination, along with the 3107 cm$^{-1}$ peak in the IR spectra, suggests these diamonds were HPHT treated before irradiation.

Owing to their extreme rarity and individuality, creating a set of matching natural-color diamonds can be quite challenging. In contrast, synthetic diamonds can demonstrate uni-formity in features and appearance due to the manufacturer's ability to control the growth conditions, defect concentrations, and the subsequent treatment parameters.

*Sally Eaton-Magaña*

**Large Pinkish Orange CVD Synthetic Diamond**

Natural diamonds with intense pink-orange color are very rare, particularly in large sizes. GIA's New York lab recently tested a pinkish orange CVD synthetic diamond, submitted by Unique Lab Grown Diamond Inc. in New York, that showed some outstanding gemological features.

This square cut weighed 5.01 ct (9.45 × 9.10 × 6.05 mm) and was color graded as Fancy Intense pinkish orange (figure 27). The color was distributed evenly throughout. A few small feathers and pinpoints were observable under the microscope at about 20× magnification, and the clarity was equivalent to SI$_1$. Infrared absorption spectroscopy revealed this was a type IIa diamond, with nitrogen concentration below the instrument's detection limit. A clear and sharp peak detected at 3123 cm$^{-1}$ is a well-known specific feature of CVD synthetic diamond. The absorption spectrum in the UV-Vis region indicated that the observed bodycolor was caused by a very strong and broad absorption band around 520 nm (figure 28). This band can be introduced to a CVD diamond during its growth. It creates a color effect similar to the one from the ~550 nm band in natural pink diamonds. There is no report of the ~520 nm band being introduced to a CVD synthetic diamond after its initial growth. In PL spectroscopy, clear emissions at 737 nm from SiV$^-$ and 503 nm from the H3 defect were recorded. In addition, strong emissions at 575 and 637 nm from NV centers were detected. As a result, this synthetic diamond showed strong orange-red fluorescence in Diamond-View imaging. Unlike other large CVD-grown diamonds, this diamond's fluorescence images hardly revealed the multiple growth layers responsible for its significant thickness. Instead, the multiple growth layers with subtle boundaries could only be detected in high-resolution cathodoluminescence (CL) images.

Based on all spectroscopic features, we believe that this CVD synthetic diamond was not treated by

*Figure 27. This CVD-grown diamond, weighing 5.01 ct and Fancy Intense pinkish orange in color, stands out among all CVD synthetics GIA has tested so far.*
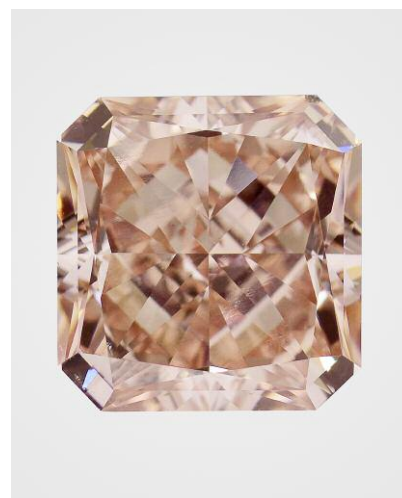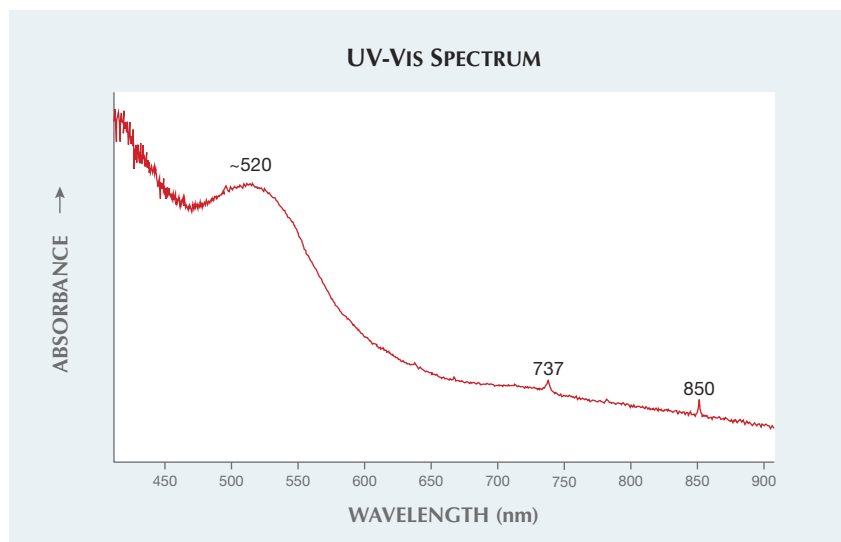
**UV-VIS SPECTRUM**

*Figure 28. The UV-Vis spectrum of this CVD synthetic revealed that its intense pinkish orange bodycolor was caused by a strong and broad absorption band around 520 nm.*
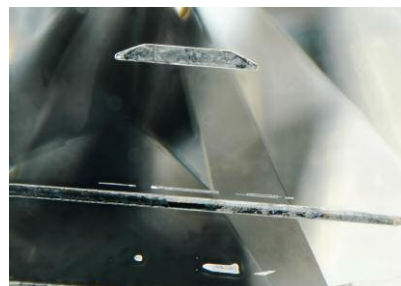


*Figure 30. The metallic flux inclusions present in the synthetic diamond. Several rod-shaped structures can be seen, as well as an inclusion with a trapezoidal shape. Field of view 4.79 mm.*

HPHT annealing after its growth for color improvement, though heating to a moderate temperature could not be entirely ruled out. The combination of size, color, and clarity made this the most remarkable CVD synthetic diamond GIA has tested so far.

*Wuyi Wang and Tom Moses*

### 15 Carat HPHT Synthetic Diamond

The Carlsbad laboratory recently examined an HPHT synthetic diamond that is now the largest faceted lab-grown diamond examined by GIA. The specimen was a cushion modified brilliant weighing 15.32 ct, with grades equivalent to $I_1$ clarity and H color (figure 29). The largest previously reported fully faceted synthetic diamonds were a 10.02 ct emerald-cut HPHT-grown (equivalent to E-color; Summer 2016 Lab Notes, pp. 195–196) and a 10.08 ct emerald-cut HPHT-grown diamond (equivalent to Fancy Deep blue; Winter 2016 Lab Notes, p. 416). The 15.32 ct synthetic contained large metallic flux inclusions (figure 30) as well as numerous fractures. Examination under crossed polarizers revealed no strain patterns, except for small strain fields around the metallic flux inclusions.

The infrared absorption spectrum showed no detectable boron or nitrogen, indicating that the sample was type IIa. DiamondView imaging did reveal blue phosphorescence, which is characteristic of boron impurities (figure 31, right), but any boron present was below the detection level of the FTIR spectrometer. PL spectroscopy

*Figure 29. This 15.32 ct cushion modified brilliant, with grades equivalent to H color and $I_1$ clarity, is the largest HPHT synthetic diamond graded by GIA.*



taken with the 514 nm laser revealed the presence of the negative silicon vacancy defect at 737 nm; the neutral nitrogen-vacancy center was also seen at 575 nm. The nickel-related doublet at 882/884 nm was seen in the 830 nm PL spectrum. EDXRF revealed the presence of iron and cobalt which, together with the nickel feature in the PL, gives insight into the flux mixture used to grow this specimen.

Due to their growth method, HPHT synthetics generally show very distinct growth patterns when examined in the DiamondView. While they can show dramatic differences in fluorescence color, these are generally seen within angular zones that radiate from the center and extend through the volume of the specimen. In contrast, CVD synthetic diamonds are grown as layers. The start/stop events of the CVD reactor result in distinct changes in diamond chemistry that are visible in DiamondView fluorescence images; the changes in fluorescence color are usually parallel due to the layered growth. Therefore, it was quite interesting to see DiamondView fluorescence patterns in which the pavilion section toward the culet far more closely resembles the layers seen in CVD growth than the cross-pattern color zoning often seen in HPHT synthetics (figure 31). The fluorescence zoning commonly found in HPHT-grown material can be seen towards
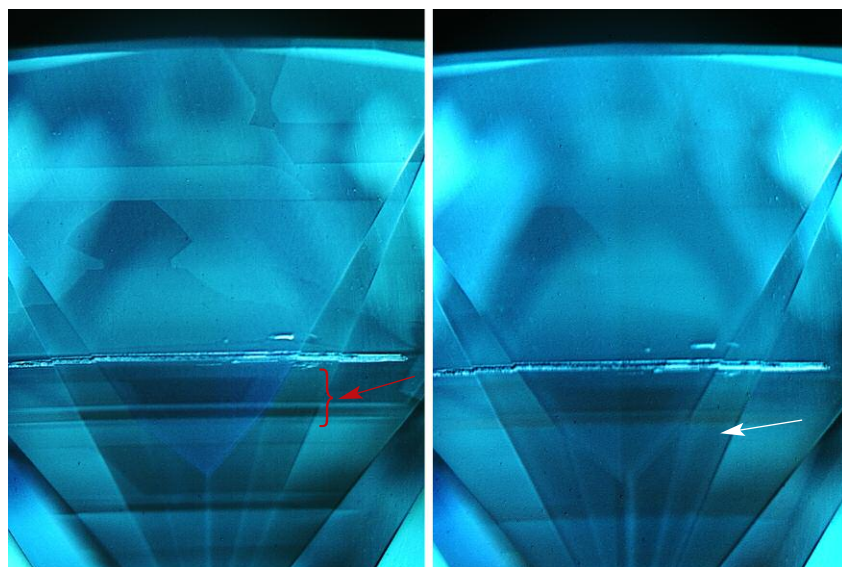
*Figure 31. Left: This DiamondView fluorescence image of the HPHT-grown diamond's pavilion shows a combination of apparent layered growth, along with the more common cross-pattern morphology seen in HPHT synthetics. The area of the pavilion shown here also indicates the region of PL mapping. The red arrow indicates the regions that showed a high concentration of nickel, silicon, and NV center defects compared to the remainder of the mapped region. Above this more heavily doped layer is the metal rod inclusion also seen in figure 30. Right: The patterning in the corresponding phosphorescence image closely resembles the fluorescence image. A thin layer of material showing orange (~580 nm) phosphorescence is indicated by the white arrow.*

the girdle section of this sample. PL mapping at liquid nitrogen temperatures was used to verify the DiamondView observations and detect the distribution of defects through the synthetic diamond (for more on the PL mapping collection technique see L.C. Loudin, "Photoluminescence mapping of optical defects in HPHT synthetic diamond," Summer 2017 *G&G*, pp. 180–189). We mapped the PL spectra of the region shown in figure 31 using 532, 633, and 785 nm laser excitations. One of the layers (red arrow in figure 31) in particular showed greatly elevated concentra-tions of nickel (as the 883/884 nm doublet; average concentration in this area was 5× greater than the average intensity of the doublet in other portions of the mapped pavilion), silicon (as the SiV$^-$ defect at 737 nm; 10× greater), and NV centers (NV$^0$ at 575 nm [2× greater] and NV$^-$ at 637 nm [2.5× greater]). This particular layer also showed orange phosphorescence in the DiamondView, assumed to be centered at approximately 580 nm (U.F.S. D'Haenens-Johansson et al., "Large colorless HPHT synthetic diamonds from New Diamond Technology," Fall 2015 *G&G*, pp. 260–279), in addition to the more common blue phosphorescence.

The specific growth process that creates the apparent layers in this HPHT synthetic is unknown, but it may be a necessary condition to grow synthetic material in such large sizes. The manufacturer may use successively larger seeds in separate growth runs or alter the pressure or temperature conditions within a single growth experiment. It should be noted that this growth feature, while layered in appearance, is quite different from CVD growth layers, which have sharp boundaries and are often differently colored. The chemistry collected on the layered portion was consistent with HPHT growth and not CVD growth; the chemistry was also consistent between the layered portion and the cross-patterned portion of growth. Therefore, a CVD seed was not used to grow this specimen. Similar layers were observed in the DiamondView images of the 10.08 ct blue HPHT synthetic (unpublished data). However, the size of this most current specimen demonstrates that the growth technologies and processes are continuing to improve and continuing to impress.

*Troy Ardon and*
*Sally Eaton-Magaña*